Pergamon

Int. J. Heat Mass Transfer. Vol. 37, No. 7, pp. 1111–1122, 1994

0017-9310/94 $6.00 + 0.00

0017-9310(93)E0029-G

Numerical simulation of Buoyancy–Marangoni convection in two superposed immiscible liquid layers with a free surface

P. WANG†, R. KAHAWITA† and D. L. NGUYEN‡

† Department of Civil Engineering, Ecole Polytechnique de Montréal, Montréal, Québec, H3C 3A7, Canada

‡ VP Recherche, Hydro-Québec, Varennes, Québec, J3X 1S1, Canada

(*Received* 24 *May* 1993 *and in final form* 27 *October* 1993)

Abstract—Buoyancy–Marangoni convection in a cavity with side heating has been studied analytically and numerically in superposed immiscible liquid layers with a free surface. The analytical results (based on an assumption of infinite aspect ratio) indicate that four different flow patterns are possible and that these results may be anticipated on the basis of the introduction of a new parameter which represents the combined effects of Marangoni forces acting at the interface between the two liquids and at the free surface. It is shown further that the new parameter is a unique thermocapillary quantity which influences the convection in the lower layer. For finite cavities, some numerical results on the mutual influence of the two layers have been presented. The numerical results obtained near the centre of the cavity are in good agreement with the results from the analytical model for sufficiently large aspect ratios.

INTRODUCTION

THERMOCAPILLARY convection in superposed immiscible liquid layers has recently begun to attract the attention of researchers due to its importance in many natural and industrial processes. Some industrial applications that involve thermocapillary forces are surface melting and alloying techniques using high power lasers, processing of ceramics and semiconductors that may frequently involve a molten and a gaseous phase. One such important application that has been commercially introduced, is the elimination of evaporation of volatile components and a reduction in thermal convection of a liquid melt by encapsulation with a protective molten material. This has resulted in a significant improvement in the quality of the final product used for the manufacture of semiconductors.

When two immiscible liquids are superposed in a rectangular cavity with differentially heated end walls, the horizontal temperature gradient induces convection due to density differences while providing an independent mechanism for its initiation. However, the effect of surface tension forces at the interface and at the free surface also plays an important role in the convective behaviour, since it influences the mechanical coupling between the two layers.

To provide an evaluation of the fundamental mechanism of natural (that is, gravity driven) and Marangoni convection, experimental and theoretical investigations in idealized geometries (rectangular cavities) has been reported [1–4] with differentially heated side walls. Oosthuizen and Paul [5] reported on an investigation into the steady state free convection heat transfer results in a closed, square container filled with a liquid and a gas based on numerical simulations. The transport phenomena in horizontal annuli formed by two circular cylinders and filled with two immiscible fluids was studied by Projahn and Beer [6].

Villers and Platten [7] reported the results of a theoretical study based on a simple analytical model for a horizontal closed cavity of infinite aspect ratio B ($B = L'/H'$, H' being the height and L' the width of the cavity). Wang *et al.* [8] presented a theoretical study based on a similar analytical model for Bénard–Marangoni heat transfer with constant heat flux and obtained the same results as those of Villers and Platten [7] for predicting the number of convective cells. The present authors [9] have numerically investigated Buoyancy–Marangoni convection in a finite cavity with side heating. Steady state solutions for the velocity and thermal fields have been obtained in the laminar regime by solving the complete two-dimensional Navier–Stokes and energy equations using the spline integration method.

Pure thermocapillary convection in two immiscible fluids has been studied numerically by Crespo *et al.* [10], however their results fail to agree with the analytical solution attributed to Doi and Koster (see Liu *et al.* [11]), except for the case $2Ma_1 = Ma_2$. Liu *et al.* [11] more recently investigated (also numerically) the convective flow induced by buoyancy and interfacial forces in a rectangular cavity of aspect ratio $B = 2$ containing two layers of immiscible fluids. They provide analytical expressions for the horizontal velocity for the two cases (rigid or free top surface) for the

NOMENCLATURE

B	aspect ratio of cavity, L'/H'
Bi	Biot number, hH'/k
g	gravitational acceleration
H_1'	height of the lower layer
H_2'	height of the upper layer
H'	height of cavity
h	fluid heat transfer coefficient
k	fluid thermal conductivity
L'	length of cavity
Ma_i	Marangoni number, equation (9)
Nu	Nusselt number
Pr	Prandtl number, μ/α
Ra	Rayleigh number, $g\beta H'^3(T_h'-T_c')/\mu\alpha$
t'	time
t	dimensionless time, $t'\alpha/H'^2$ (* signifies steady state almost attained)
T'	temperature
T_h'	temperature of vertical hot wall
T_c'	temperature of vertical cold wall
T	dimensionless temperature
u, v	dimensionless velocity components: $u_i = u_i'H'/\alpha_1$, $v_i = v'H'/\alpha_1$
u', v'	dimensional velocity components
x, y	dimensionless Cartesian coordinates.

Greek symbols

α_i	thermal diffusivity
β_i	coefficient of thermal expansion
η_i	H_i'/H'
μ_i	dynamic viscosity
ν_i	kinematic viscosity
σ_i	surface tension
Ψ	dimensionless stream function
Ω	dimensionless vorticity.

Superscript

relative quantities (layer 2 to layer 1).

case when the horizontal temperature gradient is unity.

Evidently for physically realistic cases, that is cavities with finite aspect ratios, the validity of this model is restricted to the region which is in the immediate vicinity of the cavity center. Even then, for cavities whose aspect ratios are not sufficiently large, the end effects will begin to influence the central flowfield causing significant departures from one-dimensional behaviour as will be seen later.

It is therefore not surprising that the analytical model provides a qualitative prediction for the flow and temperature fields only near the centre of the cavity with the proviso of a large enough aspect ratio B.

This effect may probably be the reason why the values of velocity at the interface and at the free surface obtained by Liu *et al.* [11] (for $B = 2$) differ from the analytical solutions for $Ma_1 = 2Ma_2$, and even for $Ma_2 = 2Ma_1$, except for smaller values of Rayleigh and Marangoni numbers. Furthermore, their computational temperature gradient at the centre of the cavity was probably not equal to unity even though they tried to impose it indirectly by using a 'perfect conductor' boundary condition at the upper and lower horizontal walls.

The oscillatory instability in thermocapillary convection has been studied [12–15] for the case of a free liquid–gas interface, since such oscillatory convection is highly undesirable for many technical processes, e.g. for crystal growth. However, transient solutions of combined buoyancy and thermocapillary convection in superposed immiscible liquid layers have not yet been reported.

The present investigation is devoted to an analysis as well as a numerical simulation of the steady flow induced in a two-layer system of immiscible liquids with an 'open' free surface under adiabatic or mixed boundary conditions. The convection is driven by the buoyancy as well as by the surface tension forces acting at the interface and at the free surface. Any deformations of the interface and the free surface have been considered negligible in the present study. A simplified analytical model for a cavity with infinite aspect ratio B has been developed for the case of an adiabatic top surface. Analytical expressions for the stream function, the horizontal velocity and for the temperature have been derived. For finite cavities, some numerical results on the mutual influence of the two layers have been presented. The flow and thermal fields have then been investigated in the laminar regime by solving the complete two-dimensional unsteady Navier–Stokes and energy equations using the spline integration method [16–22]. The numerical results obtained near the centre of the cavity are in good agreement with the results of the analytical model for sufficiently large aspect ratios B.

Finally, the influence of any heat transfer at the upper free surface on the convective flow and on the temperature field have been studied by defining a Biot number, and the results presented for mixed boundary conditions at the free surface.

GOVERNING EQUATIONS

Thermocapillary convection which is induced by a combination of density differences in a gravitational field and by surface tension gradients, is governed by the continuity equation, the two-dimensional Navier–Stokes equation and the energy equation for both fluids ($i = 1$ or 2). The non-dimensional equations in streamfunction and vorticity form (using the Boussinesq approximation for the body forces) may be

written:

$$\nabla_i^2 \Psi_i = -\Omega_i \tag{1}$$

$$\frac{\partial \Omega_i}{\partial t} + u_i \frac{\partial \Omega_i}{\partial x} + v_i \frac{\partial \Omega_i}{\partial y} = Pr_i \begin{Bmatrix} 1 \\ \bar{\alpha} \end{Bmatrix} \left[\nabla_i^2 \Omega_i + Ra_i \begin{Bmatrix} 1 \\ \bar{\alpha} \end{Bmatrix} \frac{\partial T_i}{\partial x} \right]. \tag{2}$$

For the case of heat flux through vertical opposite walls, equation (2) is replaced by:

$$\frac{\partial \Omega_i}{\partial t} + u_i \frac{\partial \Omega_i}{\partial x} + v_i \frac{\partial \Omega_i}{\partial y} = Pr_i \begin{Bmatrix} 1 \\ \bar{\alpha} \end{Bmatrix} \left[\nabla_i^2 \Omega_i + Ra_i^* \begin{Bmatrix} 1 \\ \bar{\alpha}\bar{k} \end{Bmatrix} \frac{\partial T_i}{\partial x} \right] \tag{2'}$$

and

$$\frac{\partial T_i}{\partial t} + u_i \frac{\partial T_i}{\partial x} + v_i \frac{\partial T_i}{\partial y} = \begin{Bmatrix} 1 \\ \bar{\alpha} \end{Bmatrix} \nabla_i^2 T_i \tag{3}$$

with

$$\nabla_i^2 = \frac{\partial^2}{\partial x^2} + \frac{\partial^2}{\partial y^2} \tag{4}$$

and

$$u_i = \frac{\partial \Psi_i}{\partial y}, \quad v_i = -\frac{\partial \Psi_i}{\partial x} \tag{5}$$

where $\bar{\alpha} = \alpha_2/\alpha_1$ and $\bar{k} = k_2/k_1$.

Boundary conditions

The boundary conditions for the problem are:

for $x = 0$

$$u_i = v_i = \Psi_i = 0, \quad \Omega_i = -\frac{\partial^2 \Psi_i}{\partial x^2}, \quad \text{and} \quad T_i = -0.5$$

for $x = B$

$$u_i = v_i = \Psi_i = 0, \quad \Omega_i = -\frac{\partial^2 \Psi_i}{\partial x^2}, \quad \text{and} \quad T_i = 0.5$$

for $y = 0$

$$u_1 = v_1 = \Psi_1 = 0, \quad \Omega_1 = -\frac{\partial^2 \Psi_1}{\partial y^2}, \quad \text{and} \quad \frac{\partial T_1}{\partial y} = 0 \tag{6}$$

and for $y = 1$

$$v_2 = \Psi_2 = 0, \quad \Omega_2 = \bar{\alpha} Ma_2 \frac{\partial T_2}{\partial x},$$

$$\text{and} \quad \frac{\partial T_2}{\partial y} = -Bi(T_2 - T_{amb}) \tag{6'}$$

where T_{amb} is the ambient dimensionless temperature. In the present study, an ambient temperature $T_{amb} = (T_h + T_c)/2 = 0$ was used. Most computations were performed for $Bi = 0$; however some cases where $Bi \neq 0$ when surface heat exchange was present have also been computed and the results presented.

Neglecting any deflection of the interface between the two liquids, the boundary conditions maintaining the continuity of temperature and velocity at the interface ($y = \eta_1$) are:

$$T_1 = T_2, \quad \frac{\partial T_1}{\partial y} = \bar{k} \frac{\partial T_2}{\partial y}$$

$$\Psi_1 = \Psi_2, \quad u_1 = u_2, \quad \text{and} \quad v_1 = v_2 = 0 \tag{7}$$

$$\frac{\partial^2 \Psi_1}{\partial y^2} = \bar{\mu} \frac{\partial^2 \Psi_2}{\partial y^2} - Ma_1 \frac{\partial T}{\partial x}$$

or

$$\Omega_1 = \bar{\mu} \Omega_2 + Ma_1 \frac{\partial T}{\partial x} \tag{8}$$

where Ma_1 is the interface Marangoni number and Ma_2 is the Marangoni number for the upper layer and

$$Ma_i = -\frac{\partial \sigma_i}{\partial T} \frac{(T_h' - T_c')H'}{\mu_i \alpha_i} \tag{9}$$

σ being the surface tension.

It may be noted that in immiscible two-fluid flow problems, the non-dimensional parameters are η_1, Ra_1, Ra_2, Pr_1, Pr_2, $\bar{\alpha} = \alpha_2/\alpha_1$, $\bar{\mu} = \mu_2/\mu_1$, $\bar{k} = k_2/k_1$, Ma_1 and Ma_2. Ma_1 and $\bar{k}$ arise from the non-dimensional boundary conditions at the interface.

APPROXIMATE SOLUTION

The thermocapillary convection in superposed layers is characterized by the specification of η_1, Ra_1, Ra_2, Pr_1, Pr_2, $\bar{\alpha}$, $\bar{\mu}$, $\bar{k}$, Ma_1 and Ma_2. The problem may be significantly simplified by the approximation of parallel flow as reported by Villers and Platten [7] and Wang *et al.* [8] for a closed horizontal cavity of infinite aspect ratio B. Since this implies that the lateral heat sources are located at infinity, the only velocity component present in the region of interest would be horizontal. The flow is then purely one-dimensional and the (horizontal) velocity component varies only in the vertical. The streamfunction and the temperature field may be given by

$$\Psi_i = \Psi_i(y) \quad \text{and} \quad T_i = Cx + \theta_i(y),$$

where C is a constant representing the unknown temperature gradient in the x direction.

We now define the ratio of certain physical quantities evaluated in the two layers as first introduced by Villers and Platten [7]:

$$Q_\alpha = [\rho \beta H^2]_2/[\rho \beta H^2]_1 \tag{10}$$

and

$$Q_\mu = [\mu/H]_2/[\mu/H]_1. \tag{11}$$

For the present case, if use is made of the above dimensionless parameters with $\bar{\eta} = \eta_2/\eta_1$, equation (10) and equation (11) become:

$$Q_\alpha = \bar{\alpha}\bar{\mu} Ra_2 \bar{\eta}^2 / Ra_1$$

and

$$Q_\mu = [\bar{\mu}/\bar{\eta}].$$

Q_α is related to the relative importance between the buoyancy forces in the upper and lower layers, and Q_μ is related to the viscous forces.

Thus equation (2) may be simplified to

$$\frac{d^4\Psi_i}{dy^4} = \begin{Bmatrix} 1 \\ \bar{\alpha} \end{Bmatrix} Ra_i C.$$

The following expressions are then obtained:

$$\Psi_1 = \frac{Ra_1 C}{24}[y^2(y-\eta_1)(y+\eta_1+\lambda)] \quad (12)$$

$$\Psi_2 = \frac{Ra_1 CS}{24\bar{\mu}} y'(y'-\eta_2)\left[y'^2 + (\Lambda+\eta_2)y' + \eta_2(\Lambda+\eta_2) - \frac{G_2}{2S}\right] \quad (13)$$

and

$$\theta_1 = \frac{Ra_1 C}{24}\left\{\left[\frac{(y^5-\eta_1^5)}{5} - \eta_1^2\frac{(y^3-\eta_1^3)}{3}\right] + \lambda\left[\frac{(y^4-\eta_1^4)}{4} - \eta_1\frac{(y^3-\eta_1^3)}{3}\right]\right\} \quad (14)$$

$$\theta_2 = -\frac{Ra_1 C}{24\bar{\alpha}}\left\{\frac{S}{\bar{\mu}}\left[\left(\frac{y'^5}{5} - \frac{\eta_2^3 y'^2}{2} + \frac{3\eta_2^5}{10}\right) - \Lambda\left(\frac{y'^4}{4} - \frac{\eta_2^2 y'^2}{2} + \frac{\eta_2^4}{4}\right)\right] - \frac{G_2}{\bar{\mu}}\left(\frac{y'^3}{6} - \frac{\eta_2 y'^2}{4} + \frac{\eta_2^3}{12}\right)\right\} \quad (15)$$

with

$$y' = (1-y)$$

$$\lambda = \frac{1}{\eta_1 P}[3S\eta_2^3 - 2\eta_1^2(3\bar{\mu}\eta_1 + 5\eta_2) - \eta_2 G^*]$$

$$\Lambda = -\frac{1}{2S\eta_2^2}(2\bar{\mu}\eta_1^3 + \bar{\mu}\eta_1^2\lambda + 3S\eta_2^3 - 0.5\eta_2 G_2)$$

and $S = Q_\alpha/\bar{\eta}^2$, $P = (4\bar{\eta}+3\bar{\mu})$, $G_2 = 12\overline{\alpha\mu}Ma_2/Ra_1$, $G^* = 24Ma^*/Ra_1$ and $Ma^* = Ma_1 - 0.5\overline{\alpha\mu}Ma_2$.

Here G is related to the inverse of the dynamic Bond number which is defined as $Bo = g(\rho_1-\rho_2)H'^2/\sigma$.

The velocity may be written:

$$u_1 = \frac{Ra_1 C}{24}[4y^3 - 2y\eta_1^2 + y\lambda(3y-2\eta_1)] \quad (16)$$

$$u_2 = \frac{Ra_1 C}{24\bar{\mu}}\left[-S(4y'^3-\eta_2^3) - S\Lambda(3y'^2-\eta_2^2) - \frac{G_2}{2}(2y'-\eta_2)\right]. \quad (17)$$

Evidently when sidewall heating is considered, the above expressions are independent of $\bar{k}$. This is due to the assumption that the flow is then purely one-dimensional and steady with the (horizontal) velocity component varying only in the vertical while the two horizontal walls at the top and bottom are considered insulated. In this case, the interface in effect behaves as an adiabatic boundary. For a finite cavity, the above assumptions are invalid and significant departures from the solutions based on simplifying assumptions may be expected.

It is interesting to note that the expressions of equation (12) and equation (16) for, respectively, Ψ_1 and u_1 are identical in form with the corresponding expressions for the rigid top [8, 9]. Of course the functional dependence of λ on G^*, S and $\bar{\mu}$ in the expressions will be different.

NUMERICAL PROCEDURE

Since the thermocapillary convection consists of two superposed immiscible liquid layers and one influences the other through the interface conditions, the treatment of these conditions in the computational procedure is of extreme importance. In this respect, the spline fractional step procedure (SMFS) [19] is an improvement over existing methods. The essential advantage of the technique for the present problem lies in the fact that boundary conditions containing derivatives may be easily incorporated into the solution procedure since values of first or second derivatives may be evaluated directly and maintain the same degree of accuracy when the algorithm that represents the spline approximation to the governing equations (1)–(4) is constructed. The governing matrix system obtained is always tridiagonal containing either function values or the first derivatives at the grid points. The SMFS schemes and the boundary conditions in discretized form may be obtained in direct fashion from the procedure detailed in earlier articles [9, 20–22] and will therefore not be described further.

The time dependent nonlinear coupled partial differential equations were solved by considering a 31×31, 41×41 or 81×41 grid depending on the different values of aspect ratio B. In order to accurately describe gradients that are expected to be steep in the boundary layer regions, a non-uniform grid in both the x and y directions was used. Accuracy of the solutions were verified by grid refinement. All computations were performed on a 486 based IBM compatible PC.

RESULTS AND DISCUSSION

$Bi = 0$

Pure Marangoni convection. Thermocapillary convection was observed under reduced gravity during the Spacelab D1 mission as reported by Ben Hadid and Roux [15]. In the absence of gravity, the interface tension caused by the horizontal temperature gradient is the unique source driving the thermocapillary convection.

Under these conditions, the expressions equations (12)–(17) above, simplify to the following forms:

$$\Psi_1 = -\frac{Ma^*C\bar{\eta}}{P}y^2(y-\eta_1) \tag{18}$$

$$\Psi_2 = C\left[\left(\frac{Ma^*}{2P\bar{\eta}}+\frac{\bar{\alpha}Ma_2}{4\eta_2}\right)y'(y'^2-\eta_2^2) - \frac{\bar{\alpha}Ma_2}{2}y'(y'-\eta_2)\right] \tag{19}$$

and

$$u_1 = -\frac{Ma^*C\bar{\eta}}{P}y(3y-2\eta_1) \tag{20}$$

$$u_2 = -C\left[\left(\frac{Ma^*}{2P\bar{\eta}}+\frac{\bar{\alpha}Ma_2}{4\eta_2}\right)(3y'^2-\eta_2^2) - \frac{\bar{\alpha}Ma_2}{2}(2y'-\eta_2)\right] \tag{21}$$

and

$$\theta_1 = -\frac{Ma^*C\bar{\eta}}{P}\left[\frac{(y^4-\eta_1^4)}{4}-\eta_1\frac{(y^3-\eta_1^3)}{3}\right] \tag{22}$$

$$\theta_2 = -\frac{C}{\bar{\alpha}}\left\{\left(\frac{Ma^*}{2P\bar{\eta}}+\frac{\bar{\alpha}Ma_2}{4\eta_2}\right)\left(\frac{y'^4}{4}-\frac{\eta_2^2y'^2}{2}+\frac{\eta_2^4}{4}\right) - \bar{\alpha}Ma_2\left(\frac{y'^3}{6}-\frac{\eta_2y'^2}{4}+\frac{\eta_2^3}{12}\right)\right\}. \tag{23}$$

This result clearly indicates that the velocity and the temperature distributions in the lower layer depend only on the combined Marangoni number Ma^* and the convective activity in the lower layer is weakened as the absolute value of Ma^* diminishes. For the particular case of $Ma^* = 0$, theoretically no fluid motion will arise in the lower layer, and so any heat transfer has to occur by pure conduction, the resultant temperature expression being $T = Cx$.

This result is of some practical significance since in fact (as mentioned earlier), eliminating convective flow in the lower layer is of interest in producing high quality materials obtained from diffusive crystal growth in encapsulated electronic melts. However, in order to realize this condition, i.e. diminishing Ma^* ($Ma^* = Ma_1 - 0.5\bar{\alpha}\bar{\mu}Ma_2$), an appropriate choice of the corresponding parameter values must be made. For example, values of Ma_2, μ_2 and α_2 may be chosen in order to minimise the value of Ma^*, this being a more general parameter describing the convective activity in the lower layer.

Figures 1(a) and (b) indicate, respectively, the comparisons between analytical and numerical solutions for the normalized horizontal velocities and stream function profiles (the dashed-lines represent numerical solutions) at the cavity midplane for different interface and free surface Marangoni numbers. The combined Marangoni numbers however, $Ma^* = 0$ and $\bar{\eta} = \eta_2/\eta_1 = 0.6$, $B = 5$, $\bar{\alpha} = 1$ and

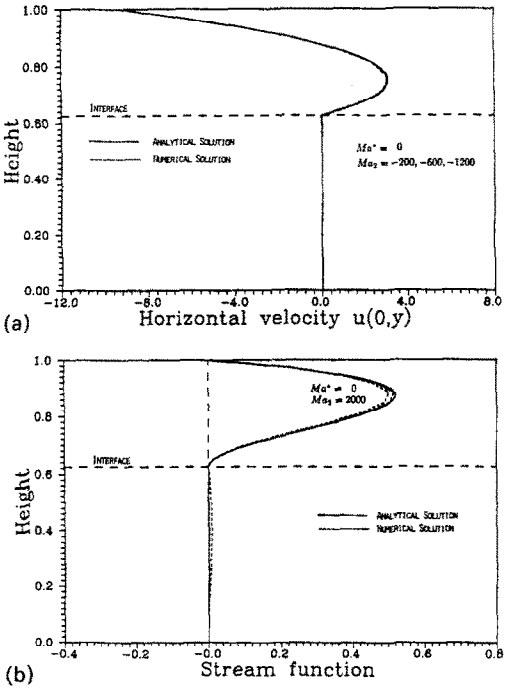

FIG. 1. (a) Comparison between analytical and numerical normalized horizontal velocity profiles at the cavity midplane ($Ma^* = 0$). (b) Comparison between analytical and numerical stream function profiles at the cavity midplane ($Ma^* = 0$).

$Q_\mu = 2$ have been maintained the same. The characteristic velocity used for all the graphs was $u^* = 100u/(Ma_2C)$, while $\Psi^* = 100\Psi/(Ma_2C)$ (all figures with the superscript * omitted), where C represents the temperature gradient. The present results used the temperature gradient at the centre point of the interface for the value of C. In fact, at the midplane, the variation of temperature gradient is very small, the mean value of the temperature gradient at the midplane deviating less than 1% from its value at the centre point for the present examples with lower Raylcigh numbers. The numerical results are in good agreement with the analytical solution. Only when $Ma_2 > 10^3$ does the numerical deviation become visually discernible in the lower layer. This is due to the end wall effects. As expected, this deviation decreases with increasing aspect ratio.

According to equation (18), only one thermocapillary cell is to be expected in the lower layer and the sense of the circulation depends on the sign (positive or negative). For example, for $Ma^* < 0$, the fluid at the interface tends to flow from the cold to the hot wall while for $Ma^* > 0$ the opposite is true.

The number of convection cells in the upper layer may be either one or two, depending on the existence of the roots to the following equation (from equation (19)) within the interval $(0, \eta_2)$:

$$\left(\frac{Ma^*}{2p\bar{\eta}}+\frac{\bar{\alpha}Ma_2}{4\eta_2}\right)(y'+\eta_2)-\frac{\bar{\alpha}Ma_2}{2}=0$$

or

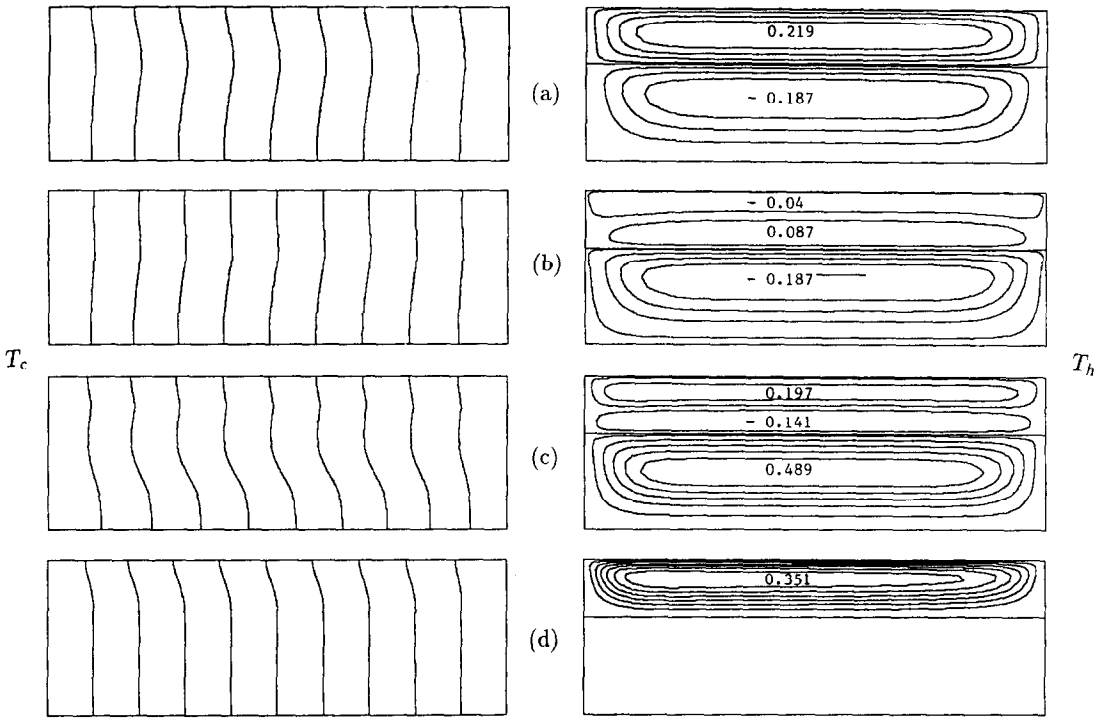

FIG. 2. Typical computed streamlines and isotherms with different cells for $\bar{\alpha} = \bar{k} = 1$, $\bar{\mu} = 1.2$ and $\bar{\eta} = 0.6$. (a) $Ma^* = -100$, $Ma_2 = 50$, (b) $Ma^* = -100$, $Ma_2 = -70$; (c) $Ma^* = 200$, $Ma_2 = 200$; (d) $Ma^* = 0$, $Ma_2 = 200$.

$$y' = -\left(\frac{Ma^*}{2p\bar{\eta}} - \frac{\alpha Ma_2}{4\eta_2}\right) \Big/ \left(\frac{Ma^*}{2p\bar{\eta}} + \frac{\alpha Ma_2}{4\eta_2}\right).$$

It is evident that, if the values of Ma^* and Ma_2 possess different signs (i.e. $Ma^* > 0$ and $Ma_2 < 0$ or $Ma^* < 0$ and $Ma_2 > 0$), there is only one convection cell in the upper layer with a direction of rotation that is contrary in sense to that in the lower layer. In fact, this fluid flow pattern may be maintained until

$$Ma_2 = \frac{2\bar{\alpha} Ma^*}{(4+3Q_\mu)\bar{\eta}}.$$

However, when

$$Ma_2 > \frac{2\bar{\alpha} Ma^*}{(4+3Q_\mu)\bar{\eta}} \quad \text{and} \quad Ma^* > 0$$

or when

$$Ma_2 < \frac{2\bar{\alpha} Ma^*}{(4+3Q_\mu)\bar{\eta}} \quad \text{and} \quad Ma^* < 0,$$

there are two cells in the upper layer.

Figures 2(a)–(d) present typical computed streamlines and isotherms with different cells for various values of Ma^* and Ma_1 the purpose of which was to illustrate the influence of these parameters on the flow field. The numerically calculated maximum and minimum stream function values Ψ_{max} and Ψ_{min} are also indicated on each graph for reference. In these figures the streamlines are equally spaced between Ψ_{max} and Ψ_{min}.

Figure 3(a) is a comparison between the analytical and numerical normalized horizontal velocity profiles at the cavity midplane for different interface and free surface Marangoni numbers with $\bar{\eta} = 0.6$, $B = 3$, $\bar{\alpha} = \bar{k} = 1$ and $\bar{\mu} = 1.2$. Again, the numerical results agree satisfactorily with the analytical solutions.

The corresponding normalized temperature profiles with $T^* = 1000T/(Ma_2 C^2)$ are shown in Fig. 3(b). Compared with the analytical solution, the computed temperature profiles are displaced along the interface velocity direction due to the effects of the end walls. This implies that the flow adjacent to the interface functions to transport hot (or cold) fluid to the center from the sides. The stronger the normalized horizontal velocity at the interface, the more evident is this displacement as shown in the figure for the case where $Ma_2 = -200$ and $Ma_1 = 50$.

Figures 4(a) and (b) illustrate the influence of the aspect ratio B on the horizontal velocity and temperature profiles at the midplane maintaining $Ma^* = 0$, $Ma_2 = -600$, $\bar{\mu} = 1.2$ and $\bar{\eta} = 0.6$ with values of $B = 2, 3, 5$, respectively. Turning to Fig. 4(a) it may be seen that in this specific case when $B > 3$ (for each layer, this implies a ratio greater than 6), the variation of the horizontal velocity profile at the midplane is in general, very small so that the solution

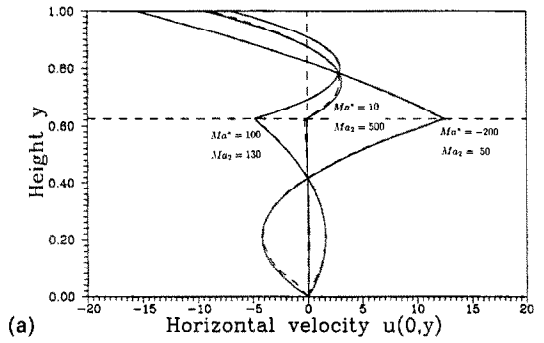

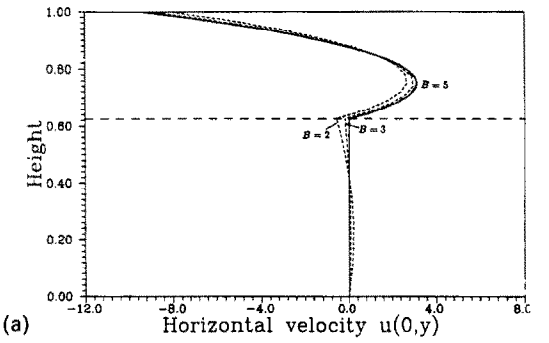

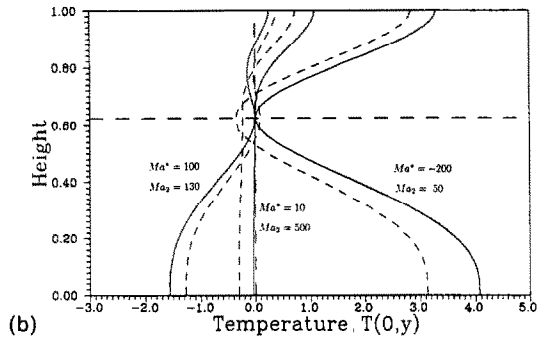

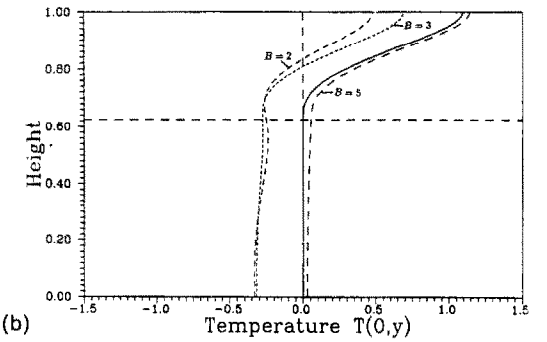

FIG. 3. (a) Comparison between analytical and numerical normalized horizontal velocity profiles at the cavity midplane for different Ma^* and Ma_2 ($\bar{\eta} = 0.6$, $B = 3$, $\bar{\alpha} = 1$ and $Q_\mu = 2$). (b) Comparison between analytical and numerical normalized temperature profiles at the cavity midplane (with the same conditions of Fig. 3(a)).

FIG. 4. (a) Influence of the ratio B on the horizontal velocity profiles at the midplane ($Ma^* = 0$, $Ma_2 = -600$ and $Q_\mu = 2$ and $\bar{\eta} = 0.6$). (b) Influence of the ratio B on the temperature profiles at the midplane ($Ma^* = 0$, $Ma_2 = -600$ and $Q_\mu = 2$ and $\bar{\eta} = 0.6$).

at the centre of the cavity may be considered as corresponding to the solution obtained using the simplified analysis for infinite aspect ratio. For the temperature profile displayed in Fig. 4(b), the difference between the numerical results and those of the analysis is still visible even for an aspect ratio of five. In fact, at higher Marangoni numbers, test computations revealed that, even when $B > 5$ (which results in a horizontal temperature gradient at the midplane which is approximately constant), the above difference remained quite noticeable.

Buoyancy-thermocapillary driven flows. Typical two layer Buoyancy–Marangoni convection flow patterns for various Rayleigh numbers and Marangoni numbers are presented in Fig. 5(a)–(g). These computations have been realised at smaller Rayleigh and Marangoni numbers in order to illustrate the influence of the parameters on the flow field. The number of cells seen in each layer depend on the values of Q_α, Q_μ, Ma^*, Ma_2 and $\bar{\eta}$. For this case, $Ra_1 = 10^3$, $Q_\alpha = 0.5$, $\bar{\alpha} = 1$, $Q_\mu = 2$, $\bar{\eta} = 0.6$ and $B = 3$ have been used.

If thermocapillary forces at the interface and at the free surface are for a particular case, negligible, i.e. $Ma_1 = Ma_2 = 0$, the convection is driven purely by buoyancy. In this case, following the definition of equation (12), for $\frac{2}{3} < Q_\alpha < 2 + Q_\mu$ there are two cells in the lower layer. As a special case, when $Q_\alpha = 2/3$ there is only one cell in each layer with the same direction of rotation as shown in Fig. 5(a), and the horizontal velocity at the interface is equal to zero. This may be immediately verified.

Figures 5(b), (c) illustrate that the secondary circulation due to the effect of the interfacial tension will be felt in the upper as well as the lower layer for $Ma^* = -50$, $Ma_2 = 200$ and $Ma^* = 100$, $Ma_2 = 200$, respectively. Figures 5(d), (e) illustrate for $Ma^* = -200$, $Ma_2 = 10$ and $Ma^* = 10$, $Ma_2 = -100$, respectively, that the secondary cell develops fully while the primary cell is weakened and disappears in the central part of the cavity, so that the circulation in each layer is of opposite sign. These results are in good agreement with the analytical predictions of equation (12) and equation (13).

The five types of convective flow as illustrated in Figs. 5(a)–(e) have been observed in a rectangular cavity containing two layers of immiscible fluids with a rigid upper surface [7, 8]. However, when the upper surface is free, the surface tension forces begin to affect the flow in the upper layer resulting in some complex flow behaviour as shown in Figs 5(f), (g). Figure 5(f) indicates the presence of two cells in each layer for $Ra_1 = 10^5$, $Q_\mu = 1$, $Ma^* = 0$ and $Ma_2 = -1200$ while in Fig. 5(g) there are three cells in the upper layer with only one cell in the lower layer for the case where $Ra_1 = 10^5$, $Q_\alpha = 2/3$, $Q_\mu = 1$, $Ma^* = -3000$ and $Ma_2 = -4000$. These are also in agreement with the analytical predictions.

Figures 6(a) and (b) present the horizontal velocity

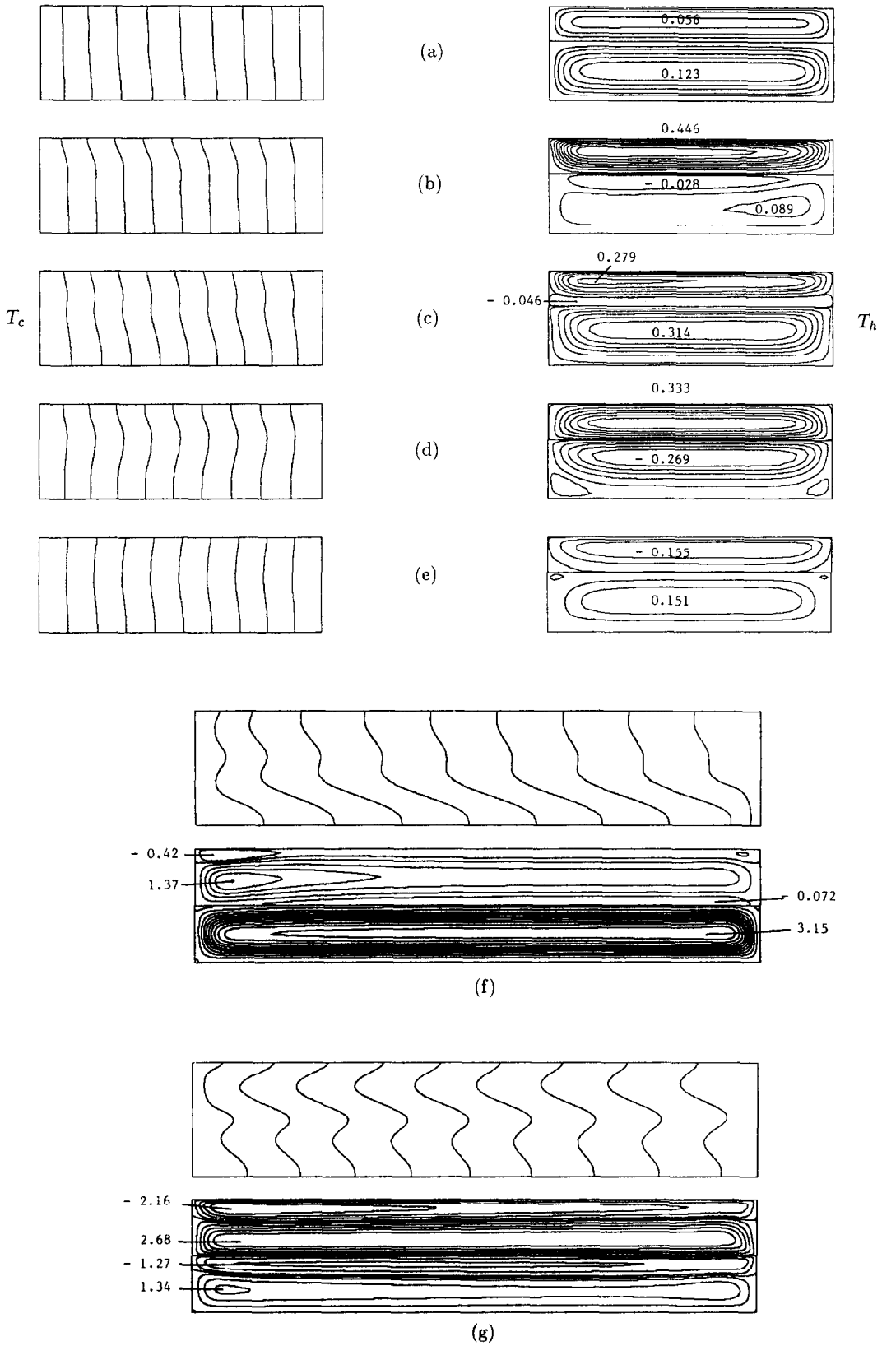

FIG. 5. Typical Buoyancy–Marangoni convection flow patterns for (a)–(e): $Ra_1 = 10^3$, $\bar{\alpha} = 1$, $Q_\mu = 2$, $\bar{\eta} = 0.6$ and $B = 3$. For (f)–(g): $Ra_1 = 10^5$, $\bar{\alpha} = 1$, $Q_\mu = 1$, $\bar{\eta} = 1$ and $B = 5$. (a) $Q_\alpha = 2/3$ and $Ma^* = Ma_2 = 0$, (b) $Q_\alpha = 0.5$, $Ma^* = -50$, $Ma_2 = 200$; (c) $Q_\alpha = 0.5$, $Ma^* = 100$, $Ma_2 = 200$; (d) $Q_\alpha = 0.5$, $Ma^* = -200$, $Ma_2 = 10$; (e) $Q_\alpha = 0.5$, $Ma^* = 10$, $Ma_2 = -100$; (f) $Q_\alpha = 0.5$, $Ma^* = 0$, $Ma_2 = -1200$; (g) $Q_\alpha = 2/3$, $Ma^* = -3000$, $Ma_2 = -4000$.

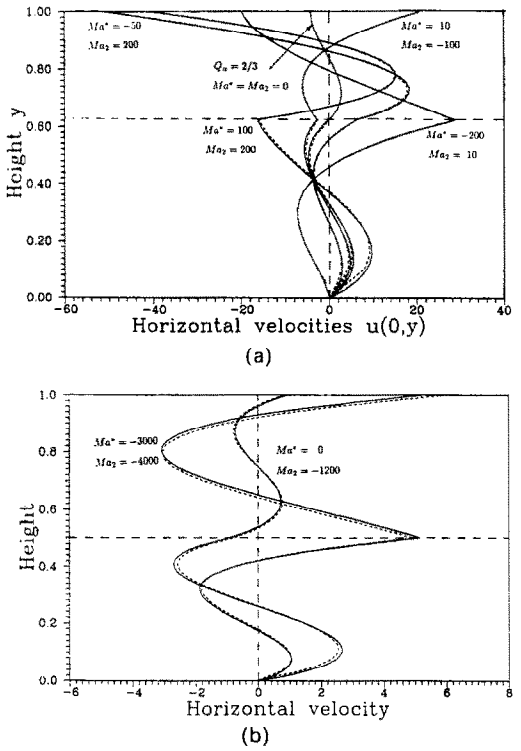

FIG. 6. (a) Horizontal velocity profiles at the midplane corresponding to Figs. 9(a)–(e). (b) Horizontal velocity profiles at the midplane corresponding to Figs. 9(f)–(g).

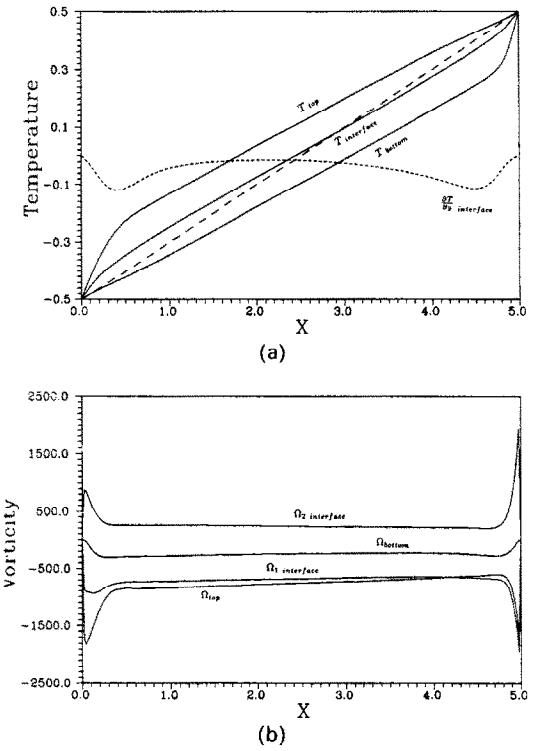

FIG. 8. (a) Temperature distributions at the top, interface and bottom of the cavity for $Ra_1 = 10^5$, $Q_\alpha = 2/3$, $Ma^* = 0$ and $Ma_2 = -1000$. (b) Vorticities at the interface, the free surface and the bottom for $Ra_1 = 10^5$, $Q_\alpha = 2/3$, $Ma_1 = -5000$ and $Ma_2 = -4000$.

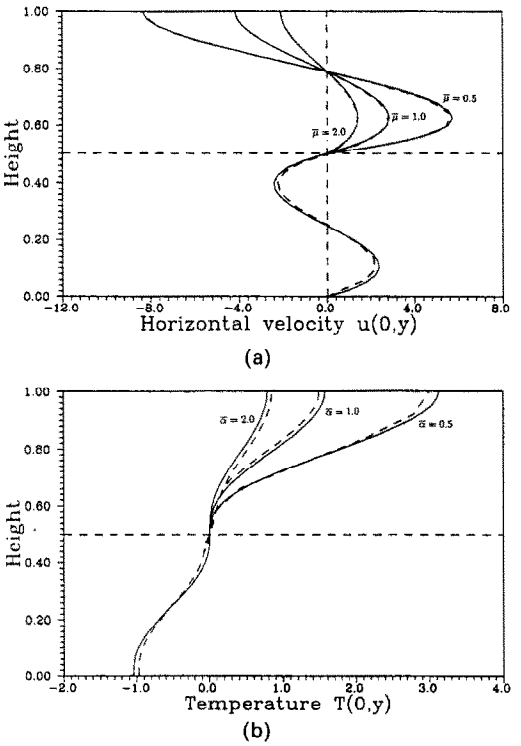

FIG. 7. (a) Influence of the value of $\bar{\mu}$ on the horizontal velocity profile at the midplane ($Q_\alpha = 2/3$ and $\bar{\mu} = 0.5$, 1.0 and 2.0). (b) Influence of the value of $\bar{\alpha}$ on the temperature profile at the midplane ($Q_\alpha = 2/3$, $Q_\mu = \bar{k} = 1$).

profiles at the midplane corresponding to the above flow patterns that go with Figs. 5(a)–(e) and Figs. 5(f)–(g), respectively. The same figure highlights the influence of the parameter Ma^* and Ma_2 on the velocity profile. The solid lines represent the values obtained from the analytical expressions equation (16) and (17). These are also in agreement with the analytical prediction. However it may be noted that for high Marangoni numbers, $Ma^* = -3000$ and $Ma_2 = -4000$, at the free surface the horizontal velocity is visually different to the analytical solution as shown in Fig. 6(b).

It is not surprising that, at the cavity midplane, the value of the horizontal velocity, $u_1(y = 2\eta_1/3)$ in the lower layer is virtually independent of Ma^* as seen in Figs. 3(a) and 6(a), (b). This conclusion may be deduced from the results in equation (16). In fact, for all cases, when the dimensionless vertical coordinate y takes on the value $2\eta_1/3$, the terms containing Ma^* vanish.

Figure 7(a) illustrates the influence of the value of $\bar{\mu}$ on the horizontal velocity profile at the midplane. In this numerical experiment, $Q_\alpha = 2/3$ was maintained while $\bar{\mu}$ was given values of 0.5, 1.0 and 2.0. The results compare favourably with the analytical solution. The following values for the parameters have been tentatively used: $Ra_1 = 10^3$, $Ma_1 = Ma_2 = 0$, $Pr_1 = Pr_2 = 10$ and $\bar{k} = \bar{\alpha} = 1$ with $B = 3$. The numerical results indicate that in the lower layer the

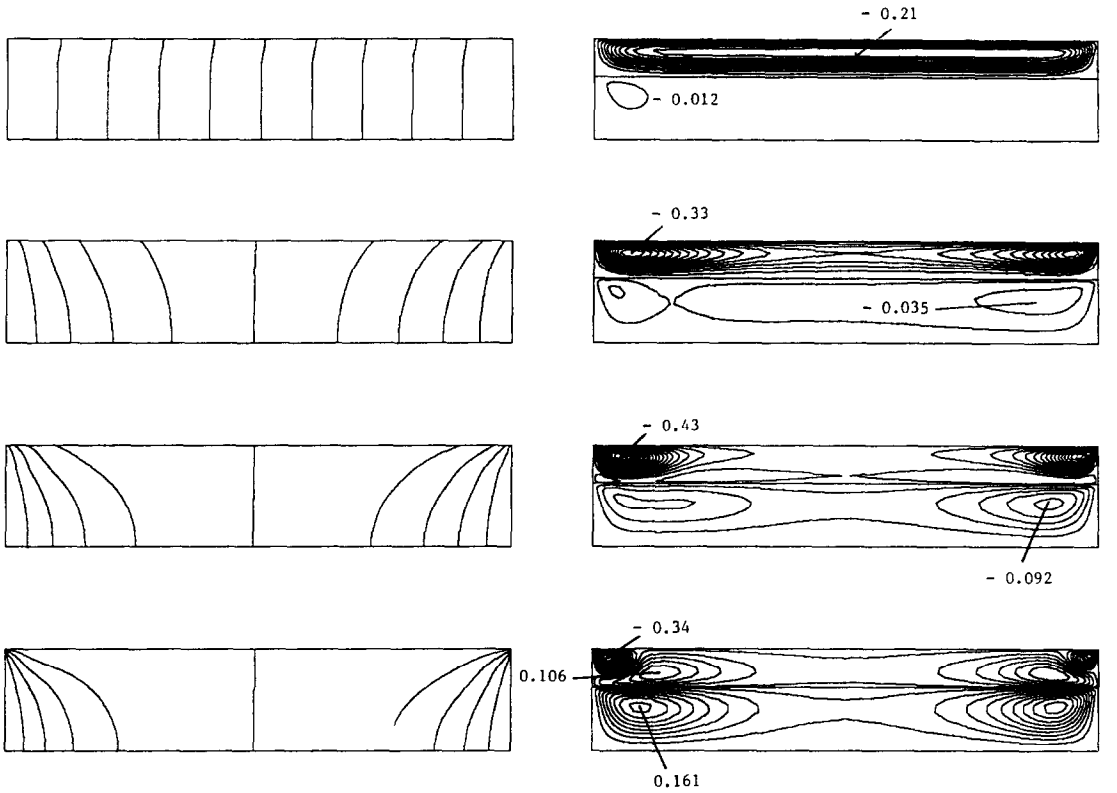

FIG. 9. Streamlines and isotherms for $Ma^* = 0$ and $Ma_2 = -200$ with $Q_\mu = 2$ and $\bar{\eta} = 0.6$ at $Bi = 0$, 2, 5 and 20.

velocity distribution is relatively unaffected. However, in the upper layer the velocities vary by a factor of $1/\bar{\mu}$. This coincides with the analytical predictions, since, in this case, there is a coefficient $1/\bar{\mu}$ in equation (15). The present numerical results are, therefore, in good agreement with those of the analytical model.

Figure 7(b) illustrates the influence of the value of $\bar{\alpha}$ on the temperature profile at the midplane with $Q_\alpha = 2/3$ while Q_μ and $\bar{k}$ are all maintained at unity. The other parameters used are the same as in Fig. 7(a). It is noted that in the lower layer the distribution of the computed temperature is relatively unaffected. However, in the upper layer the temperatures vary by a factor of $1/\bar{\alpha}$. This coincides with the analytical preditions for $Ma_2 = 0$.

Figure 8(a) presents the temperature distributions at the top, interface and bottom of the cavity for $Ra_1 = 10^5$, $Q_\alpha = 2/3$, $Ma^* = 0$ and $Ma_2 = -1000$ with $Q_\mu = \bar{\alpha} = \bar{k} = 1$. The temperature at the free surface in the upper layer is higher than that at the interface, with the interface temperature in turn being higher than that at the bottom wall. This is due to the convection in the lower layer. It is clear that in this case the heat transfer across the interface is from the lower layer to the upper layer shown by the negative vertical temperature gradient. A detailed discussion along similar lines has been presented in an earlier paper [9].

Due to the effects of different values for viscosity and the added influence of interfacial tension, the computed values of the vorticity at the interface are in general, not continuous. The vorticities at the interface, i.e. $\partial u_1/\partial y$ and $\partial u_2/\partial y$, as well as at the free surface and at the bottom for the same case of Fig. 5(g) are shown in Fig. 8(b). These vorticity distributions are almost constant with the exception of the region near the end walls and at the free surface.

Influence of Biot number at the free surface

In general, the heat exchange between the upper layer (liquid 2) and the ambient at the free surface may be quite weak. However, it was decided to further study this influence, particularly near the two sidewalls, by performing some additional numerical computations. The results indicated that the convective behaviour in the upper layer is fairly sensitive to the heat transfer at the upper free surface. For example, considering the case where $Ra_1 = 10^4$, $Q_\alpha = 0.5$, $Q_\mu = 2$ and $\bar{\eta} = 0.6$; when the Biot number was set to a value of $Bi = 0.1$ the horizontal velocity at the center of the free surface diminished by about 12%.

Figure 9 shows the streamlines and isotherms for $Ma^* = 0$ and $Ma_2 = -200$ with $\bar{\mu} = 1.2$, $\bar{\alpha} = \bar{k} = 1$ and $\bar{\eta} = 0.6$ at $Bi = 0$, 2, 5 and 20. Figure 10 shows the streamlines and isotherms for $Ra_1 = 10^4$, $Ma^* = 0$ and $Ma_2 = -200$ with $Q_\alpha = 0.5$, $Q_\mu = 2$ and $\bar{\eta} = 0.6$ at $Bi = 0$, 2, 5 and 20.

The corresponding horizontal velocity profiles to

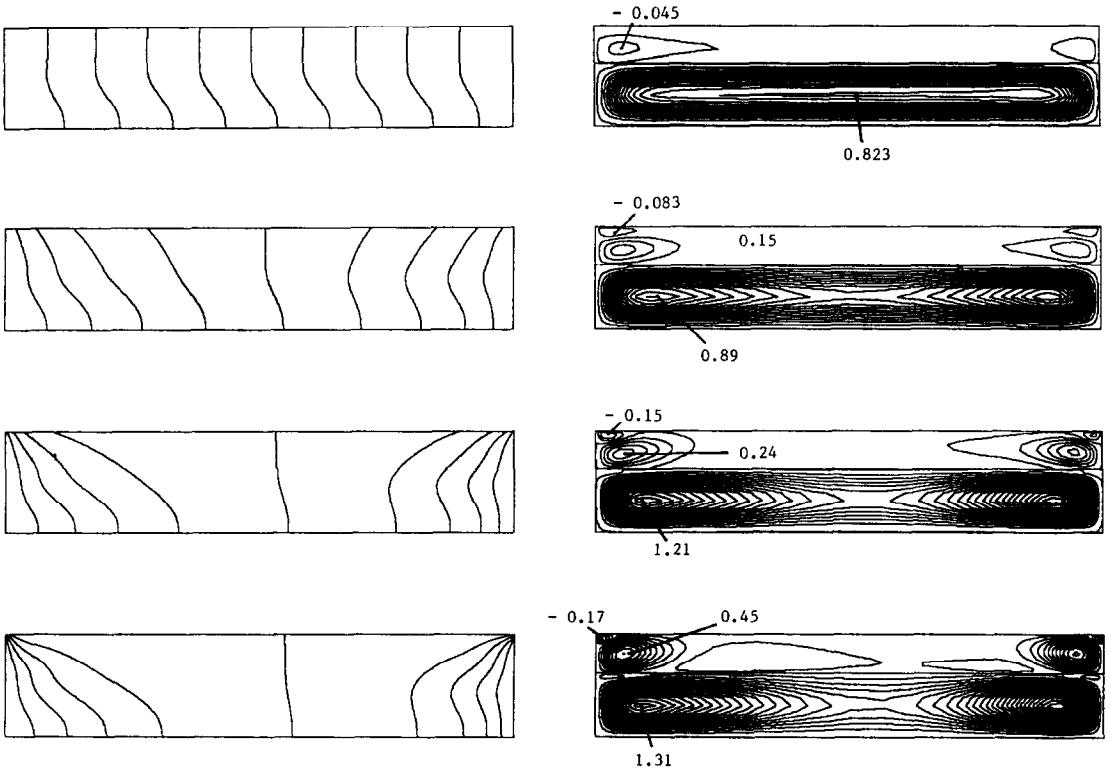

FIG. 10. Streamlines and isotherms for $Ra_1 = 10^4$, $Ma^* = 0$ and $Ma_2 = -200$ with $Q_\alpha = 0.5$, $Q_\mu = 2$ and $\bar{\eta} = 0.6$ at $Bi = 0$, 2, 5 and 20.

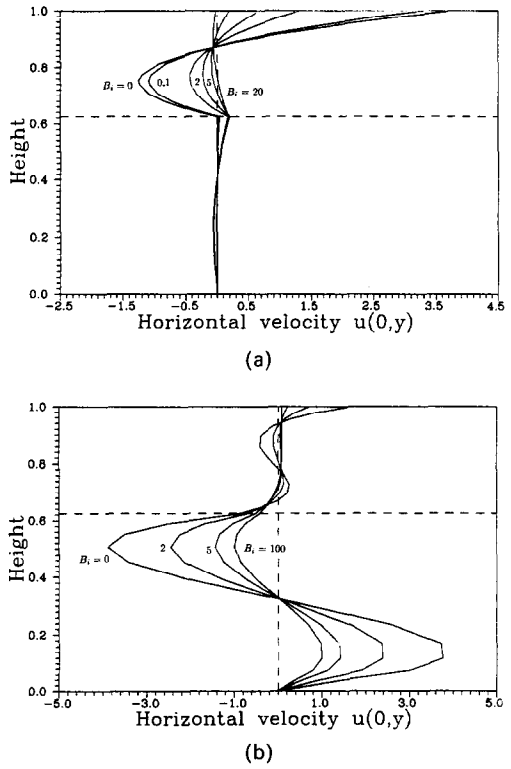

FIG. 11. (a) Dimensionless horizontal velocity profiles at the midplane of the cavity (with the same conditions of Fig. 9). (b) Dimensionless horizontal velocity profiles at the midplane of the cavity (with the same conditions of Fig. 10).

Figs. 9 and 10 at the midplane of the cavity are shown in Figs. 11(a) (b).

Clearly, the existence of any heat loss at the upper free surface (stronger near the sidewall) will result in considerable weakening of the convection in the central region of the upper layer. This may be confirmed by inspection of Figs. 11(a) and (b) which indicate the horizontal velocities and temperature profiles at the centre of the cavity. As Biot number is increased, convective activity is reduced while the temperature in the upper layer approaches ambient.

CONCLUSIONS

Marangoni convection in a two-layer cavity system with end walls maintained at a constant temperature difference has been studied numerically. An analytical solution based on the parallel flow approximation has also been presented. The computational results obtained agree qualitatively with analytical predictions when the latter are within their range of validity.

A new parameter Ma^* has been defined that uniquely characterises the velocity and temperature distributions in the lower layer. In particular, a value of $Ma^* = 0$ will result in suppression of convective activity in the lower layer under microgravity conditions, which can have useful applications to crystal pulling techniques that employ molten encapsulants.

A preliminary study of the influence of any heat

exchange at the free surface has been initiated. The results indicate that as the Biot number increases the convection in the central part of the cavity is weakened while the temperature in this region approaches the ambient value.

Current work in progress concerns the transient behaviour of the initially quiescent state to equilibrium and will be reported on shortly.

Acknowledgement—This work was supported by the Natural Sciences and Engineering Research Council of Canada under Grant Numbers OGP0008846 and OGP0036586.

REFERENCES

1. D. Villers and J. K. Platten, Separation of Marangoni convection from gravitational convection in earth experiments, *Physico-Chemical Hydrodynamics* **8,** 173–183 (1987).
2. D. Villers and J. K. Platten, Thermal convection in superimposed immiscible liquid layers, *Appl. Sci. Res.* **45,** 145–152 (1988).
3. D. Villers and J. K. Platten, Temperature dependence of the interfacial tension between water and long-chain alcohols, *J. Phys. Chem.* **92,** 4023–4024 (1988).
4. J. N. Koster, A. Prakash, D. Fujita and T. Doi, Bénard and Marangoni convection in immiscible liquid layers, *Natural Convection in Enclosures*, ASME HTD-Vol. 198 (1992).
5. P. H. Oosthuizen and J. T. Paul, Heat transfer through a closed square container filled with a liquid and a gas, ASME Paper 83-WA/HT-101, ASME Winter Annual Meeting (1983).
6. U. Projahn and H. Beer, Thermogravitational and thermocapillary convection heat transfer in concentric and eccentric horizontal, cylindrical annuli filled with two immiscible fluids, *Int. J. Heat Mass Transfer* **30,** 93–107 (1987).
7. D. Villers and J. K. Platten, Influence of interfacial tension gradients on thermal convection in two superposed immiscible liquid layers, *Appl. Sci. Res.* **47,** 177–191 (1990).
8. C. H. Wang, M. Sen and P. Vasseur, Analytical investigation of Bénard–Marangoni convection heat transfer in a shallow cavity filled with two immiscible fluids, *Appl. Sci. Res.* **48,** 35–53 (1991).
9. P. Wang, R. Kahawita and D. L. Nguyen, Numerical simulation of Marangoni convection in two superposed immiscible liquid layers, Unpublished.
10. E. Crespo del Arco, G. P. Extremet and R. L. Sani, Thermocapillary convection in a two-layer fluid system with flat interface, *Adv. Space Res.* **11**(7), 129–132 (1991).
11. Q. S. Liu, G. Chen and B. Roux, Thermogravitational and thermocapillary convection in a cavity containing two superposed immiscible liquid layers, *Int. J. Heat Mass Transfer* **36,** 101–117 (1993).
12. C. H. Chun and W. Wuest, Experiments on the transition from the steady to the oscillatory Marangoni-convection of a floating zone under reduced gravity effect, *Acta Astronautica* **6,** 1073–1082 (1979).
13. M. K. Smith and S. D. Stephen, Instabilities of dynamic thermocapillary liquid layers, *J. Fluid Mech.* **132,** 119–144 (1983).
14. D. Schwabe, U. Möller, J. Schneider and A. Scharman, Instabilities of shallow dynamic thermocapillary liquid layers, *Phys. Fluids A* **4,** 2368–2381 (1992).
15. H. Ben Hadid and B. Roux, Buoyancy- and thermocapillary-driven flows in differentially heated cavities for low-Prandtl-number fluids, *J. Fluid Mech.* **235,** 1–36 (1992).
16. S. G. Rubin and R. A. Graves, Viscous flow solutions with a cubic spline approximation, *Comput. Fluids* **3,** 1–36 (1975).
17. S. G. Rubin and P. K. Khosla, Polynomial interpolation methods for viscous flow calculations, *J. Comput. Phys.* **24,** 217–244 (1977).
18. P. Wang and R. Kahawita, Numerical integration of partial differential equations using cubic splines, *Int. J. Comput. Math.* **13,** 271–286 (1983).
19. P. Wang, Spline method of fractional steps in numerical model of unsteady natural convection flow at high Rayleigh number, *Numer. Heat Transfer* **11,** 95–118 (1987).
20. P. Wang, R. Kahawita and T. H. Nguyen, Numerical computation of the natural convection flow about a horizontal cylinder using splines, *Numer. Heat Transfer, Part A* **17,** 191–215 (1990).
21. P. Wang, R. Kahawita and D. L. Nguyen, Transient laminar natural convection from horizontal cylinder, *Int. J. Heat Mass Transfer* **34,** 1429–1442 (1991).
22. P. Wang, R. Kahawita and D. L. Nguyen, Transient natural convection with density inversion from a horizontal cylinder, *Phys. Fluids A* **4,** 71–85 (1992).